A route to sub-diffraction-limited CARS Microscopy

Willem P. Beeker,[1] Petra Groß,[2] Chris J. Lee,[1] Carsten Cleff,[2] Herman L. Offerhaus,[3] Carsten Fallnich,[2] Jennifer L. Herek,[3] and Klaus-Jochen Boller[1,*]

[1]*Laser Physics & Nonlinear Optics Group, MESA + Research Institute for Nanotechnology, University of Twente, P. O. Box 217, Enschede 7500AE, The Netherlands*
[2]*Institut für Angewandte Physik, Westfälische Wilhelms-Universität, 48149 Münster, Germany*
[3]*Optical Sciences Group, MESA + Research Institute for Nanotechnology, University of Twente, P. O. Box 217, Enschede 7500AE, The Netherlands*
**k.j.boller@tnw.utwente.nl*

Abstract: We theoretically investigate a scheme to obtain sub-diffraction-limited resolution in coherent anti-Stokes Raman scattering (CARS) microscopy. We find using density matrix calculations that the rise of vibrational (Raman) coherence can be strongly suppressed, and thereby the emission of CARS signals can be significantly reduced, when pre-populating the corresponding vibrational state through an incoherent process. The effectiveness of pre-populating the vibrational state of interest is investigated by considering the excitation of a neighbouring vibrational (control) state through an intense, mid-infrared control laser. We observe that, similar to the processes employed in stimulated emission depletion microscopy, the CARS signal exhibits saturation behaviour if the transition rate between the vibrational and the control state is large. Our approach opens up the possibility of achieving chemically selectivity sub-diffraction-limited spatially resolved imaging.

OCIS codes: (350.5730) Resolution; (300.6230) Spectroscopy, coherent anti-Stokes Raman scattering

References and links

1. H. Heinzelmann, and D. W. Pohl, "Scanning near-field optical microscopy," Appl. Phys., A Mater. Sci. Process. **59**(2), 89–101 (1994).
2. S. W. Hell, and J. Wichmann, "Breaking the diffraction resolution limit by stimulated emission: stimulated-emission-depletion fluorescence microscopy," Opt. Lett. **19**(11), 780–782 (1994).
3. T. A. Klar, S. Jakobs, M. Dyba, A. Egner, and S. W. Hell, "Fluorescence microscopy with diffraction resolution barrier broken by stimulated emission," Proc. Natl. Acad. Sci. U.S.A. **97**(15), 8206–8210 (2000).
4. E. Betzig, G. H. Patterson, R. Sougrat, O. W. Lindwasser, S. Olenych, J. S. Bonifacino, M. W. Davidson, J. Lippincott-Schwartz, and H. F. Hess, "Imaging Intracellular Fluorescent Proteins at Nanometer Resolution," Science **313**(5793), 1642–1645 (2006).
5. M. J. Rust, M. Bates, and X. Zhuang, "Sub-diffraction-limit imaging by stochastic optical reconstruction microscopy (STORM)," Nat. Methods **3**(10), 793–796 (2006).
6. B. Huang, S. A. Jones, B. Brandenburg, and X. Zhuang, "Whole-cell 3D STORM reveals interactions between cellular structures with nanometer-scale resolution," Nat. Methods **5**(12), 1047–1052 (2008).
7. R. Zenobi, "Analytical tools for the nano world," Anal. Bioanal. Chem. **390**(1), 215–221 (2008).
8. E. Rittweger, K. Y. Han, S. E. Irvine, C. Eggeling, and S. W. Hell, "STED microscopy reveals crystal colour centres with nanometric resolution," Nat. Photonics **3**(3), 144–147 (2009).
9. M. Dyba, and S. W. Hell, "Focal Spots of Size λ/23 Open Up Far-Field Fluorescence Microscopy at 33 nm Axial Resolution," Phys. Rev. Lett. **88**(16), 163901 (2002).
10. H. Ikagawa, M. Yoneda, M. Iwaki, Z. Isogai, K. Tsujii, R. Yamazaki, T. Kamiya, and M. Zako, "Chemical Toxicity of Indocyanine Green Damages Retinal Pigment Epithelium," Invest. Ophthalmol. Vis. Sci. **46**(7), 2531–2539 (2005).
11. H. H. Szeto, P. W. Schiller, K. Zhao, and G. Luo, "Fluorescent dyes alter intracellular targeting and function of cell-penetrating tetrapeptides," The FASEB Journal, 04–1982fje (2004).
12. C. J. Daly, and J. C. McGrath, "Fluorescent ligands, antibodies, and proteins for the study of receptors," Pharmacol. Ther. **100**(2), 101–118 (2003).

#113570 - $15.00 USD Received 1 Jul 2009; revised 17 Sep 2009; accepted 9 Nov 2009; published 25 Nov 2009

13. M. D. Duncan, J. Reintjes, and T. J. Manuccia, "Scanning coherent anti-Stokes Raman microscope," Opt. Lett. **7**(8), 350–352 (1982).
14. A. Zumbusch, G. R. Holtom, and X. S. Xie, "Three-Dimensional Vibrational Imaging by Coherent Anti-Stokes Raman Scattering," Phys. Rev. Lett. **82**(20), 4142–4145 (1999).
15. C. W. Freudiger, W. Min, B. G. Saar, S. Lu, G. R. Holtom, C. He, J. C. Tsai, J. X. Kang, and X. S. Xie, "Label-Free Biomedical Imaging with High Sensitivity by Stimulated Raman Scattering Microscopy," Science **322**(5909), 1857–1861 (2008).
16. C. L. Evans, E. O. Potma, M. Puoris'haag, D. Côté, C. P. Lin, and X. S. Xie, "Chemical imaging of tissue in vivo with video-rate coherent anti-Stokes Raman scattering microscopy," Proc. Natl. Acad. Sci. U.S.A. **102**(46), 16807–16812 (2005).
17. A. Nikolaenko, V. V. Krishnamachari, and E. O. Potma, "Interferometric switching of coherent anti-Stokes Raman scattering signals in microscopy," Physical Review A (Atomic, Molecular, and Optical Physics) **79**(1), 013823–013827 (2009).
18. P. W. Milonni, and J. H. Eberly, *Lasers* (John Wiley & Sons, New York, 1988).
19. Y. R. Shen, *The Principles of Nonlinear Optics* (John Wiley and Sons, New York, 1984).
20. H. Okamoto, and K. Yoshihara, "Femtosecond time-resolved coherent Raman scattering from β-carotene in solution. Ultrahigh frequency (11 THz) beating phenomenon and sub-picosecond vibrational relaxation," Chem. Phys. Lett. **177**(6), 568–572 (1991).
21. R. de Vivie-Riedle, and U. Troppmann, "Femtosecond Lasers for Quantum Information Technology," Chem. Rev. **107**(11), 5082–5100 (2007).
22. J. B. Asbury, T. Steinel, C. Stromberg, K. J. Gaffney, I. R. Piletic, A. Goun, and M. D. Fayer, "Hydrogen Bond Dynamics Probed with Ultrafast Infrared Heterodyne-Detected Multidimensional Vibrational Stimulated Echoes," Phys. Rev. Lett. **91**(23), 237402 (2003).
23. A. J. Wurzer, T. Wilhelm, J. Piel, and E. Riedle, "Comprehensive measurement of the S1 azulene relaxation dynamics and observation of vibrational wavepacket motion," Chem. Phys. Lett. **299**(3-4), 296–302 (1999).
24. S. L. McCall, and E. L. Hahn, "Self-Induced Transparency by Pulsed Coherent Light," Phys. Rev. Lett. **18**(21), 908–911 (1967).
25. B. Hein, K. I. Willig, and S. W. Hell, "Stimulated emission depletion (STED) nanoscopy of a fluorescent protein-labeled organelle inside a living cell," Proc. Natl. Acad. Sci. U.S.A. **105**(38), 14271–14276 (2008).
26. C. Ventalon, J. M. Fraser, M. H. Vos, A. Alexandrou, J.-L. Martin, and M. Joffre, "Coherent vibrational climbing in carboxyhemoglobin," Proc. Natl. Acad. Sci. U.S.A. **101**(36), 13216–13220 (2004).

1. Introduction

Optical microscopy is the workhorse of biology, providing high contrast images, often in real time, of biological processes at sub-cellular distance scales. Ultimately, it is desirable to observe interactions at the single molecule or even single functional group level. This requires resolution in the nanometer range, which is well beyond the resolution of standard confocal microscopy.

Near-field techniques, such as scanning near-field optical microscopy (SNOM) [1], have been shown to provide sub-diffraction-limited resolution images. However, these require an optical aperture, usually in the form of a tapered fiber, be placed within a few tens of nanometers of the region of interest, which typically limits the technique to surface mapping.

Recently, far-field sub-diffraction-limited resolution has been achieved by a few imaging techniques, such as: stimulated emission depletion (STED) microscopy [2, 3], photoactivated localization microscopy (PALM) [4], and stochastic optical reconstruction microscopy (STORM) [5, 6]. In the latter method the build up of photon counting statistics is used to compute emitter locations within the diffraction limited spot. STORM therefore requires an extended time to construct an image. Furthermore, STORM requires rather specialized fluorescent labels [7].

The STED technique requires fluorescent labels as well but exploits their saturable light emission; an excited state, generated by a light field, is partly depleted by an additional light field that causes stimulated emission from that state. Thereby the amount of spontaneous fluorescence is suppressed. If the additional light field possesses a node at its centre, the fluorescence process is suppressed except for a small volume around the node where the intensity is lower than the saturation intensity of the fluorescent label. Thus, resolution can be increased by increasing the intensity of the additional laser beam. Recent results show that STED can provide images with a lateral resolution of 6 nm in solids [8] or 33 nm in liquids [9].

#113570 - $15.00 USD Received 1 Jul 2009; revised 17 Sep 2009; accepted 9 Nov 2009; published 25 Nov 2009

A disadvantage of fluorescence microscopy techniques is that labels have to be introduced to the cell. The labels may influence metabolic processes in the cell, or perhaps lead to cytotoxicity [10, 11]. Furthermore, they may not attach to the correct molecule or functional group of interest [12]. There is, therefore, great interest in developing new label-free imaging techniques.

Label-free imaging modalities, such as CARS microscopy [13, 14], Stimulated Raman Scattering (SRS) microscopy [15], second harmonic generation microscopy and third harmonic generation microscopy, have demonstrated high contrast levels and video rate image acquisition times [16]. However, current implementations are unable to achieve sub-diffraction-limited lateral resolution. Unlike the STORM process, which relies on switchable fluorophores, there are no labels to be switched on or off and, unlike STED, there is no excited state to be selectively depopulated. Recently it was shown that the CARS emission can be suppressed through an interference technique [17], however, due to the linear nature of interference, this cannot be used to obtain sub-diffraction-limited resolution. This leads in to an important point: sub-diffraction-limited resolution requires nonlinearity in the optical emission process. For instance, STED works because spontaneous emission is reduced by the additional light field in a nonlinear way, which is provided by the saturation process.

To introduce sub-diffraction-limited resolution to CARS, a similar nonlinear saturation process must be identified. However, this appears to be difficult because the physical process does not involve any population inversion. A more promising approach could lie in manipulating the coherence between the ground state and the vibrational state (the so-called vibrational coherence), the presence of which is necessary for CARS emission. The analogy between CARS and STED would lie within a nonlinear process that reduces the vibrational coherence in a saturable process.

Instead of coupled-wave equations [17], we use a density matrix approach [18] to model the CARS emission process, because this traces the excitation separately from coherences, which can then be used to find intensity dependent effects, like saturation. We consider CARS emission in a configuration where two vibrational states are coupled and used to selectively inhibit CARS emission. For this situation we identified a mechanism that should enable sub-diffraction-limited resolution CARS: incoherently populating the CARS vibrational state suppresses the build-up of the vibrational coherence and reduces the CARS emission. This pre-population process is saturable and results in system behavior that is analogous to STED.

2. Theoretical framework

The level scheme of the medium and the driving light fields used in our calculations are shown in Fig. 1. The four-level system contains a ground state ($|1\rangle$), a vibrational state ($|2\rangle$), an excited state ($|3\rangle$) and a control state ($|4\rangle$). Transitions between the ground and excited states, the vibrational and excited states as well as the ground and control states are dipole allowed, while all other transitions are dipole forbidden.

First let us recall the standard description of a CARS process. The medium is illuminated by a set of three pulsed laser fields with frequencies ω_p, ω_S, ω_{pr}, called the pump, Stokes and probe, respectively. All fields are far detuned from the $|1\rangle$ - $|3\rangle$ and $|2\rangle$ - $|3\rangle$ transition frequencies. The pump and Stokes lasers are tuned such that there is a two-photon resonance between levels $|1\rangle$ and $|2\rangle$, through which $|2\rangle$ is populated. The population difference between the states $|1\rangle$ and $|2\rangle$ in combination with the pump and Stokes fields builds up the vibrational coherence. This coherence then induces two optical sidebands on the probe light frequency, one of which is the CARS emission frequency ($\omega_{cars} = \omega_p - \omega_S + \omega_{pr}$). The laser fields ω_p and ω_{pr} can be degenerate in frequency. However, for clarity, we use two different laser fields for ω_p and ω_{pr}.

#113570 - $15.00 USD Received 1 Jul 2009; revised 17 Sep 2009; accepted 9 Nov 2009; published 25 Nov 2009

To understand how the additional laser (called the control laser ω_{ctrl}), resonant with the $|1\rangle$ - $|4\rangle$ transition, influences CARS emission, we calculate the dynamics of the envelopes of the density matrix elements with the Liouville equation [19] $d\rho/dt = -i/\hbar[H,\rho] - (\Gamma_{ij}\rho_{ij})$ (see Eqs. (1-10) in the appendix for the full list of density matrix equations). The Hamiltonian, H (in dipole approximation), contains the pump, probe and Stokes laser fields, plus the control laser, with frequency ω_{ctrl}, chosen to be resonant with the $|1\rangle$ - $|4\rangle$ transition. We study the following general case (described in section 3): the incoherent population exchange rate between levels $|4\rangle$ and $|2\rangle$ is considered to be high (0.1 THz), resulting in an equal distribution of population between those two levels. Although this case seems to be special, the vibrational modes of complex organic molecules often cross-relax on a relatively short time scale [20] and therefore meet the conditions. Furthermore, we have included the effect of additional vibrational states and found that a part of the total population is transferred to these additional states, which reduces the total amount of population involved in the CARS process. However, this only affects the main result insofar that it introduces a secondary suppression of the CARS process.

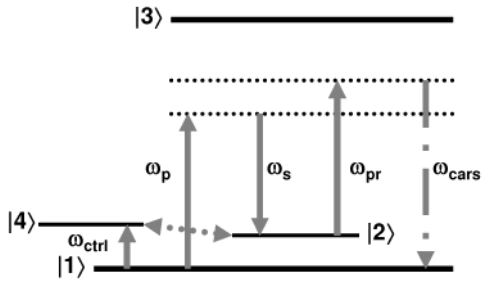

Fig. 1. Energy level diagram for CARS extended with an additional level $|4\rangle$. Level $|1\rangle$ is the ground level and initially fully occupied, $|2\rangle$ is a vibrational level of the medium, $|3\rangle$ is the excited level and level $|4\rangle$ the control level which has a fast population exchange with level $|2\rangle$. The vertical arrows between levels indicate possible transitions induced by the corresponding laser fields, which are shown far detuned from the transition $|1\rangle$ - $|3\rangle$ (ω_p, ω_S and ω_{pr}), or on resonance with the transition $|1\rangle$ - $|4\rangle$ (ω_{ctrl}). Through the nonlinear process the medium obtains a polarization at the additional ω_{cars} frequency, which is radiated by the medium.

The incident light fields E_{ij} are the sum of the pulse envelopes from the pump, Stokes, probe, and control light fields. $E_{ij} = \sum_n A_n(t)e^{i\Delta_{ij}t}$ where n = {*p, S, pr, ctrl*}. $A_n(t)$ is the Gaussian shaped pulse envelope, $\Delta_{ij} = \omega_n - \omega_{ij}$, with ω_{ij} being the transition frequency. We have assumed that there is no temporal delay between the light pulses of the pump, probe and Stokes fields. In order to prepare the state of the medium, the control pulse arrives and terminates before the onset of the other pulses.

The off-diagonal density matrix elements $\rho_{14}(t)$, $\rho_{24}(t)$, $\rho_{13}(t)$ and $\rho_{23}(t)$ act as the source terms of radiation in the Maxwell equations [18]. We obtain the full temporal development of these elements by multiplying the envelopes $\rho_{ij}(t)$ with their respective transition frequencies. The Fourier transform of this provides the spectrum of the emitted radiation.

We choose energy levels, detunings and pulse durations that are typical for CARS emission processes from molecules (specifically, we do not choose values for a particular molecule so that our results are quite general) and in view of the complexity of the system, we use numerical solutions (fourth-order Runge-Kutta algorithm with a fixed step size). The $|1\rangle$ - $|3\rangle$ transition frequency is set to 1000 THz (~300 nm, ~33,000 cm^{-1}), and the $|1\rangle$ - $|2\rangle$ frequency to 47 THz (6.4 μm or 1550 cm^{-1}). Likewise, we choose a $|1\rangle$ - $|4\rangle$ transition frequency of 97 THz (3.1 μm or 3200 cm^{-1}), which is close enough to $|2\rangle$ to allow for a high nonradiative population transfer rate of 0.1 THz. The detuning for the pump, Δ_p, and Stokes, Δ_S, light fields from the $|1\rangle$ - $|3\rangle$ and $|2\rangle$ - $|3\rangle$ transition, respectively, are both taken as –353

#113570 - $15.00 USD Received 1 Jul 2009; revised 17 Sep 2009; accepted 9 Nov 2009; published 25 Nov 2009

THz to provide two-photon resonance with the |1⟩ - |2⟩ transition. The detuning for the probe Δ_{pr} is taken as −200 THz on the |1⟩ - |3⟩ transition. To allow for coherent population transfer between |1⟩ and |2⟩, the total lifetime of state |3⟩ is taken to be in the order of picoseconds, the lifetime of |2⟩ and |4⟩ is taken to be in the order of nanoseconds, while the coherence lifetimes between states is of the order of picoseconds (see e.g., refs [21–23].). All the laser pulse durations τ are set to 2 ps ($1/e^2$) except for the control pulse, which is set to 35 ps and arrives 60 ps in advance. The simulations extend over 100 ps in steps of 2.5 attoseconds.

First, the stability and accuracy of the numerical solutions were confirmed by reproducing well-known results (see Fig. 2) such as the various Raman shifted and Rayleigh scattered fields. The population dynamics found in these initial simulations confirm that the two-photon resonance of the pump and Stokes light fields generates vibrational coherence, which radiates CARS emission as a sideband of the probe field. The nature of this process also indicates how to suppress CARS emission: if the system is prepared with equal initial populations in the |1⟩ and |2⟩ states, this will suppress the build-up of coherence on that transition, thus preventing CARS emission as well. In this approach, it is the purpose of the control laser to achieve this by first populating state |4⟩, which is chosen such that |2⟩ is rapidly populated via non-radiative mechanisms, before the arrival of the pump, Stokes, and probe pulses.

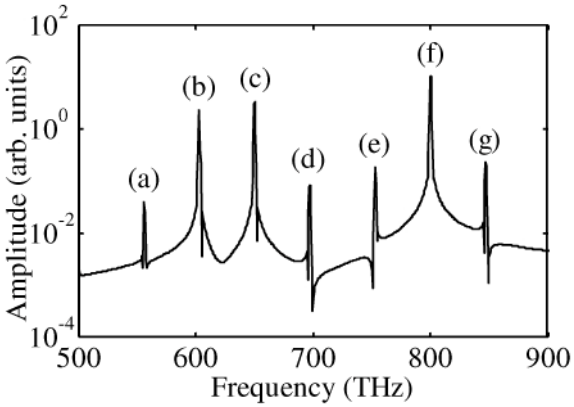

Fig. 2. Calculated emission spectrum. The features are (a) the Stokes shifted field of ω_S, (b,c,f) Rayleigh scattering of ω_S, ω_p and ω_{pr}, respectively, (d) the anti-Stokes shifted field of ω_p, (e) Coherent-Stokes-Raman scattering (CSRS) and (g) Coherent Anti-Stokes Raman Scattering (CARS) of ω_{pr}.

3. Results and discussion

In this section, we discuss how the intensity of the control pulse modifies the CARS emission intensity. This control pulse populates |4⟩ to a density that is related to the energy of the pulse as can be seen in Fig. 3a. Due to the fast redistribution between |4⟩ and |2⟩, the population density of |2⟩ closely follows that of |4⟩. This process saturates for a critical pulse area [24], given in terms of the maximal Rabi frequency multiplied by the pulse duration, which is about 100 radians in the displayed case. The preparation of the medium by the pre-pulse frustrates the build up of ρ_{12}, thus suppressing CARS emission, as can be seen in Fig. 3b. These calculations show that CARS emission can be suppressed to a maximum of 99.8% compared to the normal intensity of CARS emission. Furthermore, we observed that the intensity of all other non-linear emission processes (Fig. 2, peaks (a), (d) and (e)) are similarly suppressed.

We found that the saturation intensity, which we define as the intensity of the control beam at which the CARS signal drops to one half of its maximum value [25], corresponds to a 25% reduction of the ground state population density achieved by the control pulse prior to

#113570 - $15.00 USD Received 1 Jul 2009; revised 17 Sep 2009; accepted 9 Nov 2009; published 25 Nov 2009

the CARS process. For comparison with required values for the absolute intensities, a ground state depletion of 50% and population inversion of vibrational states of a liquid biological sample has been demonstrated by Ventalon *et al.* [26], through direct excitation by a mid-IR laser. Considering the reported pulse duration, pulse energy, and the bandwidths of the vibrational states, we estimate that the populations of their ground state and first vibrational state become equalized at intensities in the order of 70 GW/cm^2 during a 100 fs pulse. However, it should be noted that the pulse area of the control laser is more important than the intensity, thus, in our calculations, where a 35 ps pulse duration is considered, the intensity is just 200 MW/cm^2. This is well below the threshold for multiphoton ionization and excitation in the mid-infrared. A considerable advantage of this excitation scheme is that the molecule remains in its electronic ground state.

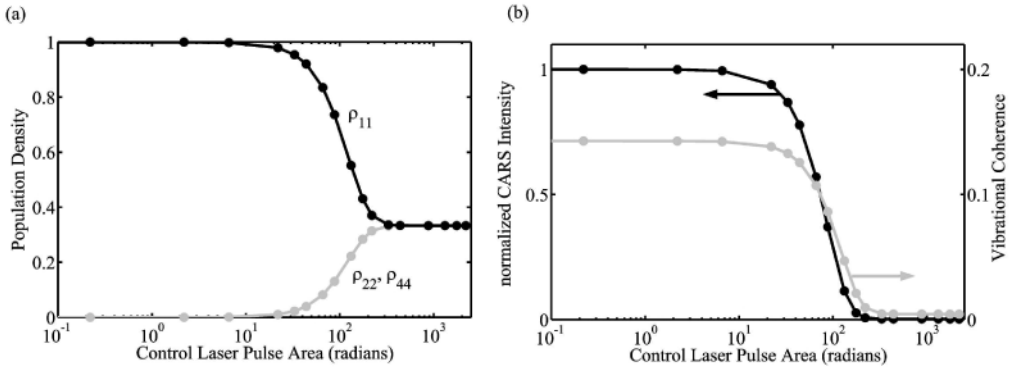

Fig. 3a. Typical population densities after application of the control pulse. For large pulse areas, a significant fraction of the ground state population is transferred to |4⟩ and, via non-radiative transitions, to |2⟩. Figure 3b. vibrational coherence ρ_{12} (grey) and corresponding intensity of CARS emission (black) after application of the control pulse. The vibrational coherence is suppressed and CARS emission is saturated by the control pulse beyond a pulse area of ~100 radians.

The resolution can be estimated by considering an experimental setup wherein the control laser illuminates the sample with a donut mode, focused to a diffraction-limited spot. The CARS signal from the node with an area defined by where the control laser's intensity is lower than the saturation intensity is not suppressed. Emission from outside the node is suppressed by 99.8%. The resolution can then be considered to be defined by the radius of the node when the signal contribution from within the node is greater than the signal contribution from outside the node. From our numerical results, we derive an upper limit to the improved resolution of approximately λ/(22*NA) where NA is the numerical aperture of the imaging system and λ is the wavelength of the probe beam.

We conclude from our calculations that sub-diffraction-limited resolution images can be obtained by extending the standard CARS microscopy setup with a control laser beam with a node at its center (a donut shaped beam), resonant with the |1⟩ - |4⟩ transition and with an intensity above the saturation level of the vibrational transition of interest. Then, the node at the center leaves the CARS process unaffected in a sub-diffraction-limited space around the center of the common focus, whereas CARS emission from that area outside the node is suppressed. The measured CARS signal is then attributed to this sub-diffraction-limited region, where the intensity is less than the saturation intensity.

4. Conclusion

We have demonstrated a route to obtain sub-diffraction-limited resolution in CARS microscopy, for which we have presented density matrix calculations for a four-level system. An intense control laser beam can be used to suppress CARS emission, when the control laser

#113570 - $15.00 USD Received 1 Jul 2009; revised 17 Sep 2009; accepted 9 Nov 2009; published 25 Nov 2009

pre-populates an additional vibrational state that is non-radiatively coupled to the vibrational state and probed by the CARS process. For neighboring vibrational states that are coupled with high transitional probabilities, as can routinely be found for aqueous biological samples, a saturation process analogous to that of STED is observed. Our calculations, based on typical parameters for molecular transitions used in CARS microscopy, showed that high saturation levels of up to 99.8% could be obtained, which provides an upper limit on the improved resolution of ~λ/(22*NA) of the probe beam. The required intensities for the control beam, which depend on the pulse area, span a range from 200 MW/cm^2 through to 100 GW/cm^2, depending on the pulse duration, seem tolerable because the molecules remain in their electronic ground state.

5. Appendix

The differential equations of all density matrix elements are:

$$\dot{\rho}_{11} = -\frac{i}{2}\left(\chi_{13}\rho_{13} - \chi_{13}^{*}\rho_{13}^{*} + \chi_{14}\rho_{14} - \chi_{14}^{*}\rho_{14}^{*}\right) + \rho_{22}R_{21} + \rho_{33}R_{31} + \rho_{44}R_{41} \tag{1}$$

$$\dot{\rho}_{22} = -\frac{i}{2}\left(\chi_{23}\rho_{23} - \chi_{23}^{*}\rho_{23}^{*} + \chi_{24}\rho_{24} - \chi_{24}^{*}\rho_{24}^{*}\right) + \rho_{33}R_{32} + \rho_{44}R_{41} - \rho_{22}R_{24} - \rho_{22}R_{21} \tag{2}$$

$$\dot{\rho}_{33} = \frac{i}{2}\left(\chi_{13}\rho_{13} - \chi_{13}^{*}\rho_{13}^{*} + \chi_{23}\rho_{23} - \chi_{23}^{*}\rho_{23}^{*}\right) - \left(R_{31} + R_{32} + R_{34}\right)\rho_{33} \tag{3}$$

$$\dot{\rho}_{44} = \frac{i}{2}\left(\chi_{14}\rho_{14} - \chi_{14}^{*}\rho_{14}^{*} + \chi_{24}\rho_{24} - \chi_{24}^{*}\rho_{24}^{*}\right) + \rho_{33}R_{34} - \rho_{44}R_{41} - \rho_{44}R_{42} + \rho_{22}R_{24} \tag{4}$$

$$\dot{\rho}_{12} = \frac{i}{2}\left(\chi_{13}^{*}\rho_{23}^{*} - \chi_{23}\rho_{13} + \chi_{14}^{*}\rho_{24}^{*} - \chi_{24}\rho_{14}\right) - \Gamma_{12}\rho_{12} \tag{5}$$

$$\dot{\rho}_{13} = \frac{i}{2}\left(\chi_{13}^{*}\left(\rho_{33} - \rho_{11}\right) + \chi_{14}^{*}\rho_{34}^{*} - \chi_{23}^{*}\rho_{12}\right) - \Gamma_{13}\rho_{13} \tag{6}$$

$$\dot{\rho}_{14} = \frac{i}{2}\left(\chi_{14}^{*}\left(\rho_{44} - \rho_{11}\right) + \chi_{13}^{*}\rho_{34} - \chi_{24}^{*}\rho_{12}\right) - \Gamma_{14}\rho_{14} \tag{7}$$

$$\dot{\rho}_{23} = \frac{i}{2}\left(\chi_{23}^{*}\left(\rho_{33} - \rho_{22}\right) + \chi_{24}^{*}\rho_{34}^{*} - \chi_{13}^{*}\rho_{12}^{*}\right) - \Gamma_{23}\rho_{23} \tag{8}$$

$$\dot{\rho}_{24} = \frac{i}{2}\left(\chi_{24}^{*}\left(\rho_{44} - \rho_{22}\right) + \chi_{23}^{*}\rho_{34} - \chi_{14}^{*}\rho_{12}^{*}\right) - \Gamma_{24}\rho_{24} \tag{9}$$

$$\dot{\rho}_{34} = \frac{i}{2}\left(\chi_{13}\rho_{14} + \chi_{23}\rho_{24} - \chi_{14}^{*}\rho_{13}^{*} - \chi_{24}^{*}\rho_{23}^{*}\right) - \Gamma_{34}\rho_{34} \tag{10}$$

With R_{ij} being the decay rate through spontaneous emission from state i to j and Γ_{ij} the decoherence rate between states i and j.

#113570 - $15.00 USD Received 1 Jul 2009; revised 17 Sep 2009; accepted 9 Nov 2009; published 25 Nov 2009